American Journal of Engineering and Applied Sciences

Original Research Paper

Landslide Susceptibility Mapping with GIS in Nagi Dada Area of Panauti Municipality, Kavrepalanchwok District: A Comparison Between AHP and FR Method

[1]Arju Bhattarai, [1]HimLal Shrestha, [2]Asim Timalsina, [3]Sujan Bista, [3]Kishor Rimal and [3]Anushka Gyawali

[1]Department of UNIGIS, University of Salzburg, Austria, Nepal
[2]Department of Geology, Trichandra Multiple Campus, Nepal
[3]Department of Geology, Tribhuwan University, Nepal

Article history
Received: 07-06-2024
Revised: 11-06-2024
Accepted: 05-07-2024

Corresponding Author:
Arju Bhattarai
Department of UNIGIS,
University of Salzburg,
Austria, Nepal
Email: arjubhtrai@gmail.com

Abstract: Landslide Susceptibility Maps (LSM) are useful for both development planning and disaster management. Currently, LSMs are primarily created using GIS and remote sensing techniques. Landslide susceptibility mapping relies heavily on selecting and weighting causative elements based on their impact on slope instability. GIS is useful for calculating static parameters such as slope and aspect, as well as generating landslide susceptibility maps. The different primary data were collected for Kinematic analysis of the study area. The lesser Himalayan rocks are represented by phyllites, pelitic schists, white quartzite, meta carbonates, graphitic schists, laminated quartzite, and garnetiferous schists. This study serves in preparing LSM covering 4 wards of Panauti municipality known as the Nagi Dada area. LSM can produced using various methods using qualitative, hierarchical, and quantitative methods. In this study, 2 methods Analytical Hierarchical Process (AHP) method and the Frequency Ratio (FR) method are used and the efficacy of both methods is compared. The resulting insights hold the potential to inform evidence-based decision-making, empower stakeholders, and pave the way for sustainable urban planning in the Panauti area. The study area is classified as a tourist area with parks, gardens, paragliding, and further infrastructure development underway. The registered landslide areas in the area are ward number 4, 8, 3, and 12 of the Panauti municipality. In this situation, landslide susceptibility mapping is crucial because it identifies the area that is susceptible to landslides by ranging from low to high chances of a landslide occurring in the given area. The landslide susceptibility would serve as the foundation for the Panauti municipality's future planning. ArcGIS Pro is used for calculating static parameters such as slope and aspect, as well as generating landslide susceptibility maps. All together 10 causative factors i.e., slope, slope aspect, curvature, LULC, lithology, distance from River, distance from drainage, distance from the fault, TWI, and precipitation are used in producing LSM. The LSM map was categorized into 5 susceptible indexes i.e., very high, high, moderate, low, and very low. The area is susceptible places for landslides and the scenario of mitigation measure failure was also observed in the area. Kinematics analysis was done in the major three landslides and the failure chances in percentage were calculated. A success rate of 85.2% was achieved with LSM using the FR method whereas 75.4% was achieved using the AHP method which is of very good accuracy.

Keywords: Landslide, LSM, AHP, FR, Geology, Lesser Himalayan

Introduction

Landslides, one of the biggest natural hazards, cause yearly property damage in direct and indirect expenses. Landslides are the movement of a mass of rock, debris, or earth down a slope (Cruden, 1991). Landslides can move in several ways, including flowing, sliding, toppling, or falling. In general,

landslides are caused by a combination of geo-environmental factors, i.e., many of which include 2 or more different movement types (Varnes, 1978). Landslides have frequently caused property and infrastructure damage and occasionally resulted in human losses. According to literature, between 1990 and 2005, landslides accounted for 5% of all natural hazards worldwide. These numbers will likely increase, in the future due to seismic activities, climate change-induced rainfall levels, and human activity on fragile slopes (Kanungo *et al*., 2009). In mountainous areas across the world, landslides have taken countless lives and resulted in enormous financial damages. Up to 100,000 people have died in the worst landslides (Li, 1992). The Nepal Himalaya is the longest section of the Himalayas. It occupies the central position and extends all over Nepal. The location of the study area is given in the map as shown in Fig. (1).

Panauti is a relatively small municipality in the Kavrepalanchok district of the Bagmati zone of the central development region. The municipality lies 32 km east of Kathmandu and immediately south of Banepa municipality. The main source of income here is agriculture. The study area is comprised of 4 wards within the Panauti municipality, with spatial extent between 27°32'-27°38' north latitude and 85°24'-85°30' east longitude. The Kavre area's rocks can be classified into 2 types: Crystalline high-grade metasedimentary rocks and Kathmandu Nappe (complex) (Stöcklin and Bhattarai, 1997). Similarly, while studying the geology of the Kavre area the Bhimphedi group, divided by the Chak-Rosi thrust and the Benighted slate of the upper Nuwakot group comprise the lithological units dispersed throughout the research region. The lithological units constitute the eastern closure of the NW-SE and dip southward. The primary joint sets in the rock masses are 3-4, including the joint parallel to foliation. The discontinuity characteristics show that the rocks have a smooth to rough surface with a soft filling aperture, indicating they are blocky. The rock bulk is rigid, indurated, and almost entirely new. Toppling failures, plane failures, and stable and unstable wedges all affect the slopes (Paudel and Tamrakar, 2013). The primary causes of large-scale landslides on central Nepal's highways are the significant hydrothermal alteration in the lesser Himalayas during the Main Central Thrust (MCT) and, consequently, clay mineralization in sliding zones of large-scale landslides. Additionally, this study indicates that slope failure in the lesser Himalayas of Nepal during the monsoon is primarily caused by large-scale landslides (Hasegawa *et al*., 2009). The local tectonic activity has caused these rocks to fracture and fold. The region's tectonic activity has resulted in folding and faulting. Sedimentary rocks, such as sandstones, siltstones, and shales, were deposited during the Jurassic and Cretaceous periods. Metamorphic rocks, such as gneisses, granites, and schists, are products of the intense heat and pressure that go into the development of mountains (Stöcklin and Bhattarai, 1997). The area is prone to landslides and rock falls because of the steep terrain and deteriorating rocks. In 2014, there was a landslide in the nearby Sindhupalchowk area that caused substantial damage and killed several people (Van Der Geest and Schindler, 2016). With the kinematics of past landslides in an area, geologists and engineers can create hazard maps that delineate zones prone to landslide activity. These maps serve as valuable tools for land-use planning, infrastructure design, and emergency preparedness (Rusydy *et al*., 2019). Additionally, the variety of conditioning factors in slope units is ignored, which leads to the incompleteness of the input variables in LSP modeling. In this study, LSP modeling is constructed from the slope units retrieved by the MSS approach using the internal variations of conditioning factors inside a slope unit, which are represented by the descriptive statistics aspects of mean, standard deviation, and range (Chang *et al*., 2023). This study's large-scale geological mapping and site-specific kinematic analyses in various spatial domains confirmed that, despite the competent lithology (quartz, gneiss, and quartzite) within this 180 m stretch, there is a high likelihood of both plane and wedge failures due to gentler and unfavorably oriented planar discontinuities concerning the available resources (Ghosh *et al*., 2014).

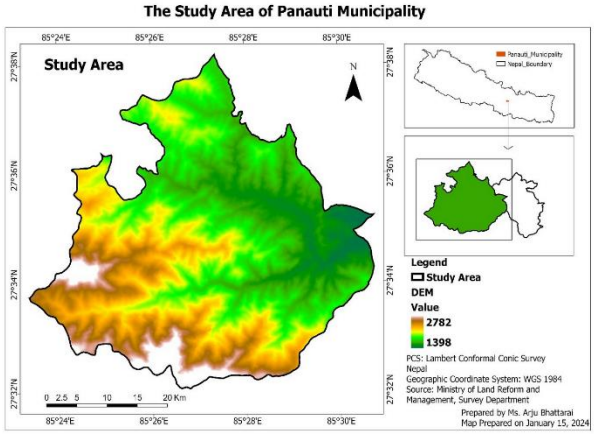

Fig. 1: Location map of the study area

Materials and Methods

Spatial datasets play a pivotal role in advancing the accuracy and efficacy of landslide susceptibility mapping through the integration of the AHP method and the FR method. In the AHP method, spatial data sets are instrumental in delineating criteria such as slope, land cover, and lithology, which are crucial factors influencing landslide occurrences. These datasets enable the quantification of pairwise comparisons and the assignment of weights to each criterion, providing a geospatial foundation for decision-makers (Saaty and Vargas, 2001). Similarly, in the FR method, spatial datasets are fundamental for identifying conditioning factors associated with landslide occurrences. The synergy between spatial datasets and both AHP and FR methods fosters a comprehensive understanding of landslide susceptibility, thereby supporting informed decision-making and proactive measures for landslide risk mitigation and management (Mondal and Maiti, 2013).

Grid Size and Coordinate System Projection Used

In this study, all the datasets required for the study area were maintained at 12.5 m of resolution. DEM and its derivatives, distance raster datasets, geology, precipitation, and landslides inventory polygon datasets were maintained to 12.5 m resolution by applying the resampling tool available in ArcGIS Pro.

Image Processing

Before compositing and mosaicking, sentinel-2 level-2 A bands were reduced to the area of interest, resampled to 12.5 m pixels using ArcGIS Pro, and saved in ENVI format. Resampled images were composited into a single image using ArcGIS Pro software. Next, the composited band picture from the preceding procedure was utilized to mosaic 2 image layers into a single continuous image. Two DEM Image layers were overlaid to provide continuous DEM images for the study region.

Data Processing

Clipping and masking is the process of pulling data from a specified area of interest. The clip function aligns the scope of one geographical layer with another. All datasets in this study were cut to cover a larger study area. Rasterization is the process of turning vector data (points, lines, and polygons) into raster form (pixels). The polyline and polygon conversion tool is essential for converting these data types to raster. At present, the landslide factors and landslide files were rasterized using the polygon to raster tool, with a cell size of 12.5 m. The raster object is created through resampling, which adjusts the spatial resolution of the input raster by developing rules for aggregating or interpolating data over new pixel sizes. This procedure is referred to as resampling. ArcGIS Pro has 4 types of resampling functions: Nearest neighbor, majority algorithm, bilinear interpolation/bilinear interpolation plus, and cubic convolution. This study resampled DEM and precipitation datasets using closest neighbor resampling, with output cell size set to sentinel 2 level 2 A (12.5 m). The fastest interpolation technique is nearest neighbor, which preserves cell beginning values and is suitable for discontinuous data such as land use classification (Yalcin, 2007). The spatial analyst toolbox is used for reclassifying raster data. This tool allows users to modify the values of a raster dataset based on specified ranges or criteria. For the landslide susceptibility mapping, a total of 10 factors are used after reading multiple papers and fieldwork i.e. Slope, slope aspect, curvature, stream, road, rainfall, lithology, TWI, LULC, and distance from the fault.

Kinematic Analysis Using DIPS

For the kinematic analysis of slope failure data were collected from joints of exposure of landslide in the field and the failure analysis is done using DIPS software. Gather geological and geotechnical data related to the slope. This includes information on joint orientations, spacing, persistence, roughness, and any other relevant geological features. The joint orientation data (dip and dip direction) into DIPS. This data is typically collected in the field using a compass. To calculate the failure; joint datasets (joints having similar orientations) are collected. The field data are given as input data to dips and it analyzes the data giving the failure percentage.

Analytical Hierarchy Method

The Analytic Hierarchy Process (AHP) is a systematic and structured decision-making method that has found application in landslide susceptibility mapping. AHP involves the decomposition of a complex decision problem into a hierarchy of criteria and alternatives, allowing for a comprehensive and organized assessment. In landslide susceptibility mapping, various factors such as slope, land cover, soil type, and precipitation contribute to the overall vulnerability of an area to landslides (Mondal and Maiti, 2013).

The landslide susceptibility map was derived using the weighted overlay method and categorized into 5 susceptible classes namely, Very Low (VL), Low (L), Moderate (M), and High (H) (Kumar and Anbalagan, 2016). This method depends on the weightage given by expertise according to Tables (1-2), in this research the possible weightage is given by studying multiple literatures, field work, and consultation with expertise.

Table 1: Matrix of pairwise comparison

C	A1	A2	…	An
A1	a11	a12	…	a1n
A2	a21	a22	…	a2n
:	:	:	…	:
Am	am1	am2	…	amn

Table 2: The basic scale of preference between two variables for a pairwise comparison matrix in the AHP method (Saaty and Vargas, 2001)

Importance rank	Degree of preference	Explanation
1	Equal importance	Both criteria provide equal contributions to the objective
3	Moderately importance of one over another	Experienced and judgment marginally to somewhat prefer one set of criteria over another
5	Strongly importance	Judgment and experience essentially favor one criterion over another
7	Very strongly importance	Experience and judgments are strongly favored over another and its dominance is shown in practice
9	Extremely importance	The evidence favoring of one criterion over another is the highest degree probable of an affirmation
2, 4, 6, and 8	Intermediate values between two adjacent judgments	Used to represent compromising between preferences in weight 1, 3, 5, 7 and 9
Reciprocals are	Opposites	Used for inverse comparison

In this model, the consistency index, known as the Ratio of Consistency (CR), is for indicating the probability that the matrix judgments were generated randomly. The consistency ratio is stated as valid if it is less or equal to 10% (Saaty and Vargas, 2001):

$$CR = CI/RI \quad (1)$$

Here *RI* stands for random index which is given in Table 4 whereas *CI* is calculated by the given formula:

$$CI = (\lambda\, max - n)/(n-1) \quad (2)$$

where, λ *max* is the principal or largest eigenvalue of the matrix and could be calculated easily from the matrix and *n* is the matrix number (Saaty and Vargas, 2001).

Landslide Susceptibility Index from AHP Method

The weighting/rating values for all contributing factors and factors' classes were calculated in the AHP Excel sheet. From the literature review, the general equation for creating an LSI map is shown below (Kumar and Anbalagan, 2016):

$$LSI = \sum_{i=1}^{n} Ri * Wi \quad (3)$$

where,

LSI = Landslide susceptibility index
Ri = Rating class of each layer
Wi = Weights of each landslide causative factor

In this research, the (Eq. 3) formula was applied for generating an LSI map by using the weighted overlay function available in ArcGIS Pro. Later on, the susceptible classes were divided into 5 different classes i.e., Very high, high, Moderate, low, and very low (Hasekioğulları and Ercanoglu, 2012)

Frequency Ratio Model

The Frequency Ratio (FR) method is a statistical technique commonly employed in landslide susceptibility mapping. This method relies on analyzing the spatial distribution of landslides about different conditioning factors to assess the likelihood of future landslide occurrences. The key premise behind the frequency ratio method is that certain environmental variables or factors contribute more significantly to landslide susceptibility (Yalcin *et al*., 2011). To apply the frequency ratio method, various conditioning factors such as slope, land cover, lithology, and rainfall are considered. The process involves calculating the ratio of the frequency of landslides within a specific class of each factor to the overall frequency of landslides in the study area. The resulting ratios provide a measure of the relative importance of each factor in influencing landslide occurrence. For instance, if areas with a certain slope range experience landslides more frequently compared to the overall average, the frequency ratio for that slope class would be greater than 1, indicating a higher susceptibility. Conversely, a frequency ratio of less than 1 implies a lower susceptibility (Ehret *et al*., 2010). Frequency Ratio (FR) is one of the bi-variate statistical approaches of landslide susceptibility assessment which is based on observed relationships between landslide distribution and each causative factor related to landslides. This technique can be used to determine the spatial correlation between the site of landslides and the explanatory elements for them (Yalcin, 2008). Based on their association with the occurrence of landslides, the FR for each subclass of individual causative factor is determined. The frequency of the sub-class of each causative factor can be calculated by using the following formula (Ehret *et al*., 2010):

$$Frequency\ Ration = (Mi/M)(Ni/N) \quad (4)$$

where,

Mi = Number of pixels with landslides for each subclass conditioning factor, *M* = total number of landslides pixels in the study area

Ni = Number of pixels in the subclass area of each factor and *N* = total number of pixels in the study area

Landslide Susceptibility Index from Frequency Method

The landslide susceptibility index was computed by adding up the raster datasets generated from the application of frequency ratio based on Eq. (4):

$$LSI = Fr1 + Fr2 + Fr3 + \ldots + Frn \quad (5)$$

where, *LSI* = landslide susceptibility index, *Fr* = rating of each factor's class.

After that using raster calculator tool in ArcGIS Pro was used to generate the landslide susceptibility index. LSI maps into 5 various landslide susceptibility categories: Very low, low, moderate, high, and very high (El Jazouli *et al*., 2019).

Validation

The Receiver operating characteristic (Roc) curve is a useful tool in the field of landslide susceptibility mapping since it provides a quantitative assessment of the model's ability to predict landslides. This curve aids in determining the optimal balance between accurately predicting landslide occurrences and reducing false alarms. The roc curve can be used by researchers to assess the susceptibility model's dependability, optimize parameter values, and improve overall forecast accuracy.

Therefore, the ROC curve serves as a crucial tool in guiding the development and validation of landslide susceptibility mapping models, contributing to more effective and reliable hazard assessment and mitigation strategies (Hoo *et al*., 2017).

Table 3 gives the categorization of the ROC curve on the basis of the value obtained.

Table 3: The categorization of ROC curve value

AU-ROC curve value	Category
0.9-1.0	Excellent
0.8-0.9	Very good
0.8-0.7	Good
0.7-0.6	Satisfactory
0.6-0.5	Poor

Results

From the landslide inventory map, the location of the landslide is traced that the maximum landslide is near the built-up areas the reason may be road construction, mining, etc. From the landslide location data sets, the training and testing data are separated for the validation process the landslide inventory map representing training and testing data is shown in Fig. (2).

Similarly, the polygon datasets of landslide in Fig. (3) give the total area of the study area covered by landslide. From the field investigation and landslide inventory map from Google Earth. The inventory, the area of the landslide was found to be ranged from 9.2-44446.34 m^2. More landslide was found in built-up areas and near road areas however, various triggering factors have equal importance in inducing landslides.

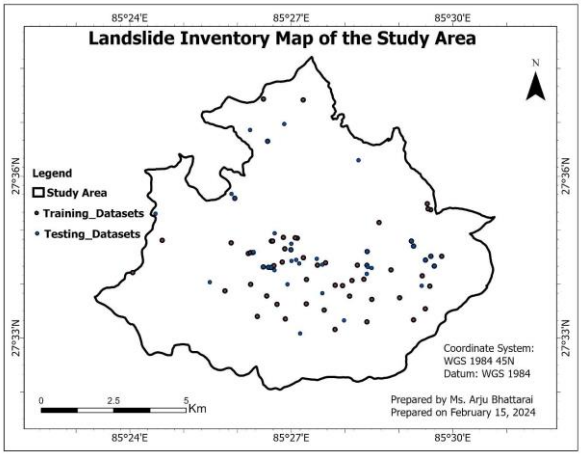

Fig. 2: Map indicating testing and training dataset of the study area

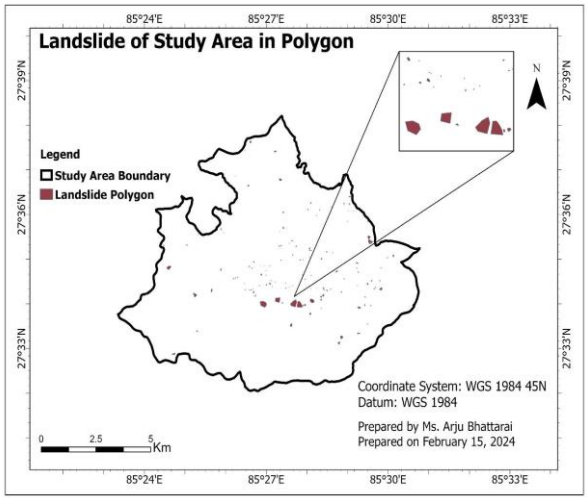

Fig. 3: Map after digitizing landslide area in Polygon

Kinematics Analysis

For kinematics analysis, three major areas of landslide are taken from each landslide 50-60 data is collected using a Brunton compass, and the DIPS Software is used which provides us with the chances of failure in the given area so as to provide suggestions and mitigation measures. In the field study the major landslide area of concern is taken as shown in Fig. (4). The results of Kinematic analysis of the study area using DIPS software are given in Fig. (4).

Kinematic analysis aims to identify critical failure surfaces within the landslide mass. These surfaces represent the pathways along which sliding or failure is most likely to occur and are important for predicting potential landslide hazards. Hence the kinematic analysis is formed in the field investigation. The result of kinematic analysis performed in the three locations to study possible failures in the study area.

The detail of the kinematic analysis is given in Table 4.

Slope

Slope significantly impacts surface and subsurface hydrology, as well as terrain stability. Landslide susceptibility estimates rely heavily on this characteristic. Moreover, the literature review suggests steep slopes are very prone to a landslide so, in this research the Slope map was prepared covering 5 classes: Very low/flat (0-15°), low (15-30°), moderate (30-45°), high (45-60°) and very high (>60°) as shown in Fig. 5.

Slope Aspect

A slope's aspect refers to its orientation relative to the north. The literature review suggests slope aspect affects solar heating, soil moisture, and air dryness.

The slope aspect affects the stability of the terrain by regulating soil moisture and vegetation growth through sunshine exposure. For susceptibility analysis, aspect maps are divided into nine classes: N, NE, E, SE, S, SW, W, NW, and Flat. Landslides in different slope aspects are given in Table 7 the slope aspect of the study area is shown in Fig. 6.

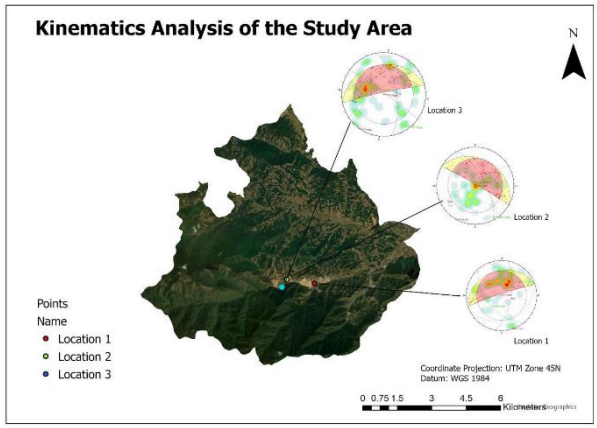

Fig. 4: The map representing the point location of the data collection for kinematic analysis

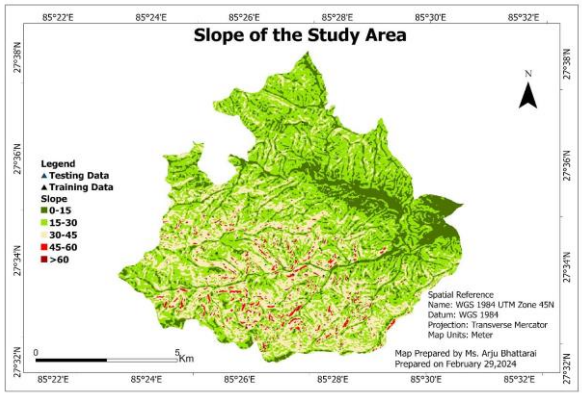

Fig. 5: The map representing the slope of the study area

Table 4: Details of possible failure in the Landslide prone area

Location	Slope dip	Slope dip direction	Friction angle	Failure type	Failure in %
1	86°	342	30°	Wedge failure	12.0
				Planar failure	6.0
				Planar failure (All)	12.0
				Flexural toppling	18.0
				Direct toppling	14.0
2	86°	342	30°	Wedge failure	19.4
				Planar failure	2.0
				Planar failure (All)	26.0
				Flexural toppling	8.0
				Direct toppling	8.0
3	87°	30	30°	Wedge failure	23.7
				Planar failure	5.7
				Planar failure (All)	44.2
				Flexural toppling	25.0
				Direct toppling	7.6

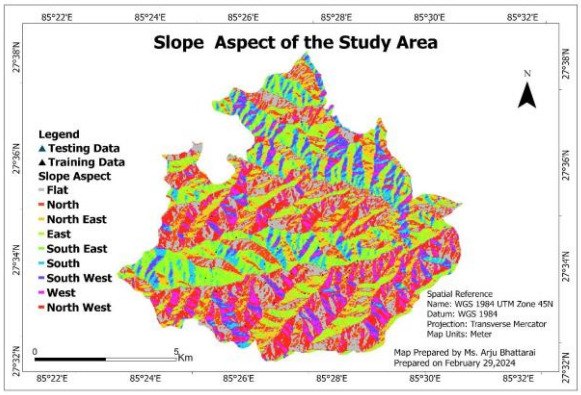

Fig. 6: Slope aspect map of the study area

Lithology

Rocks of the Kathmandu complex and Phulchauki group were found in the study area. Mainly metasandstone, phyllite, and slate were the dominant rocks present in the exposed area.

The lithology of the study area consists of all 6 forms, i.e., Pulchauki formation, Chitlang formation, Tistung formation, Chandragiri formation, and Sopyang formation of the Phulchauki group. The detailed map showing the formation present in the study area is shown in the Fig. 7.

Road

The road network can significantly influence the occurrence of landslides. Building roads on unstable terrain increases the risk of landslides. Figure 8 shows the distribution of landslide events at various distances from the road network.

Fault

Fault distance is crucial in landslide occurrences as it directly influences the potential for slope instability. The proximity of a fault to a slope can amplify the risk of landslides due to the geological and tectonic forces associated with fault activity. Closer fault distances often increase the slope's stress and strain, heightening the likelihood of slope failure and triggering landslides. As shown in Fig. 9 Euclidean distance of the existing fault is classified into three classes i.e., 0-1300, 1300-2600, and greater than 2600 meters, and the presence of landslide in each class is given in Table 8.

Drainage

Landslides were frequently observed along the research area's stream. The location of the landslide from the stream was deemed a geomorphology-related causal element. Field observations show that slope failure occurs more frequently along streams due to groundwater migration and toe undercutting. A distance to drainage map was created for landslide activity analysis and susceptibility evaluation as shown in Fig. 10.

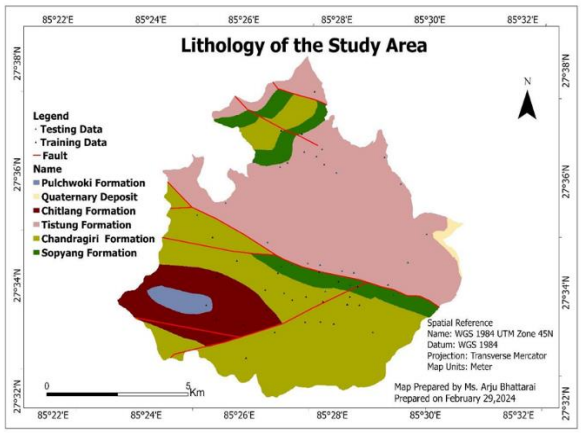

Fig. 7: The map representing the lithology of the study area

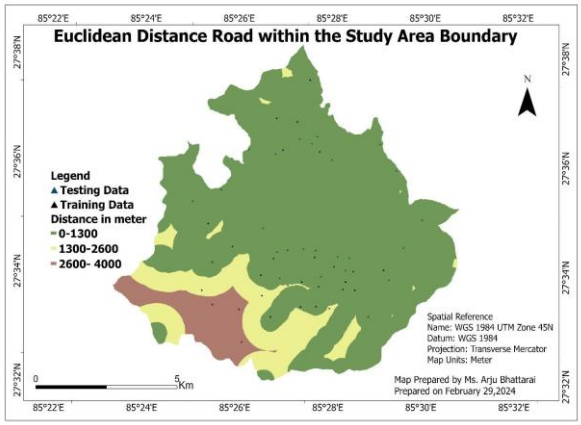

Fig. 8: The map representing Euclidean distance of road with the study area boundary

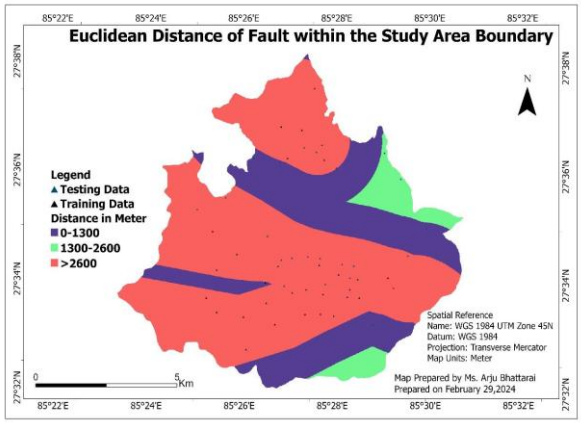

Fig. 9: The map representing Euclidean distance of fault within the boundary of the study area

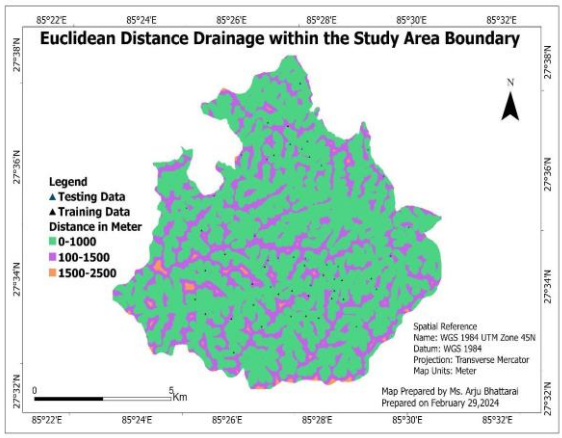

Fig. 10: The map representing Euclidean distance of drainage within the boundary of the study area

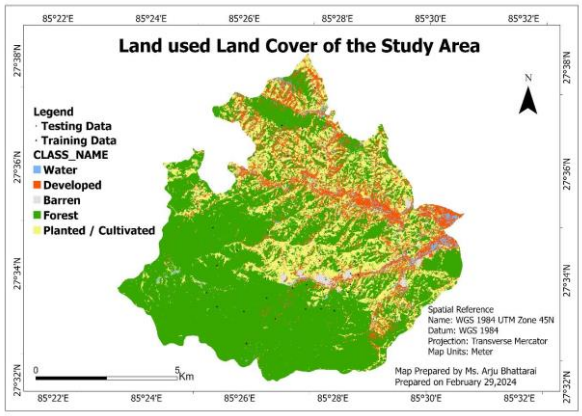

Fig. 11: The map representing the study area's land use land cover map

Land Use Land Cover

Land cover always controls the landslide process. Well-forested slopes are less prone to landslides. Land cover always controls the landslide process. Slopes in forest areas are always less prone to landslide occurrence whereas unmanaged built-up areas and cultivation also drainage like water stream could induce landslide. In Fig. 11 LULC map of the study area is divided into 5 classes i.e. Water, developed, barren, forest, planted/ cultivated.

The Kappa coefficient of the LULC map is 0.865 which means 85% accuracy and P_accuracy 93%.

Rainfall

Rainfall is an extrinsic parameter it had been used with a susceptibility map for producing landslides in the study area. For the average annual rainfall data preparation 13 years' data in the format of CSV file was used for 6 rainfall stations as shown in Fig. 12 and it was categorized into 5 classes i.e., 1028-1038, 1038-1048, 1048-1058, 1058-1068, 1068-1080 in mm.

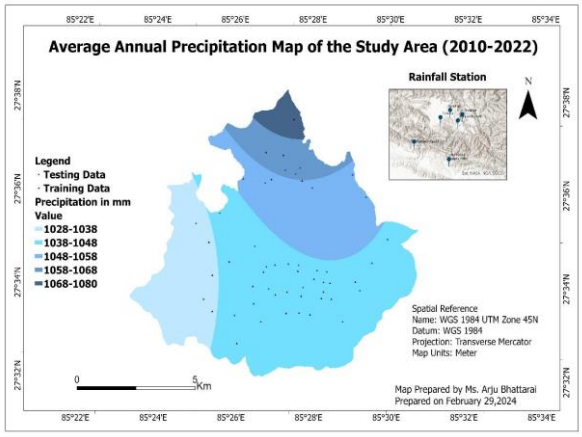

Fig. 12: Average annual precipitation map of the study area (2010-2012)

Topographic Wetness Index (TWI)

TWI from DEM is a widely used method for assessing soil moisture, with altering TWI values influencing both moisture and species (Bhandari and Upreti, 2015). The distribution of landslides across various TWI classes is clearly apparent in Fig. 13 and it is classified in 4 categories i.e., 0-7, 7-12, 12-17, 17-23. Maximum landslide is seen in range 0-7 where the landslide area is 292500 m^2.

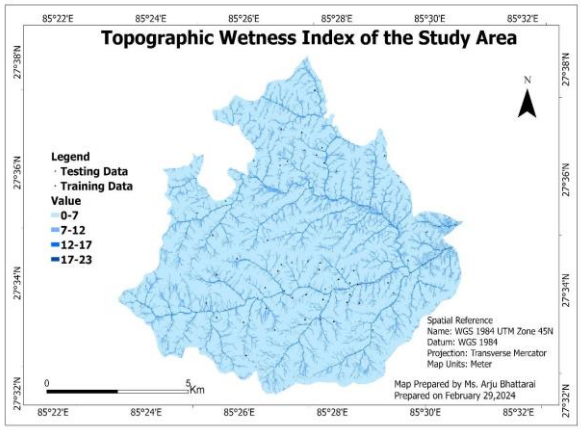

Fig 13: Map representing the topographic wetness index of the study area

Slope Curvature

Curvatures, along with other parameters, influence water flow in and out of slopes, making them crucial for studying landslides this study focused on profile curvature. A profile curvature map was created, depicting both concave and convex profiles as shown in Fig. 14. Similarly, the table shows the landslide coverage in each class.

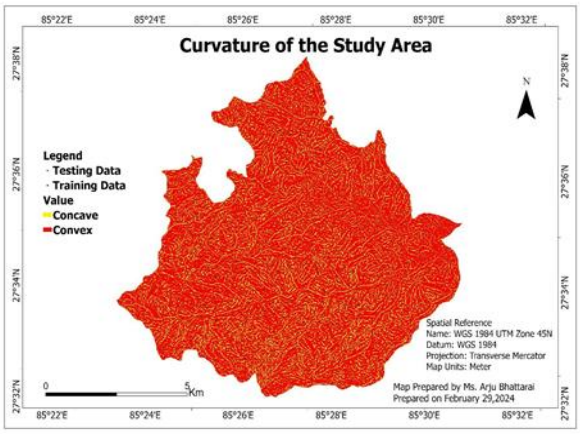

Fig. 14: Map showing the curvature of the study area

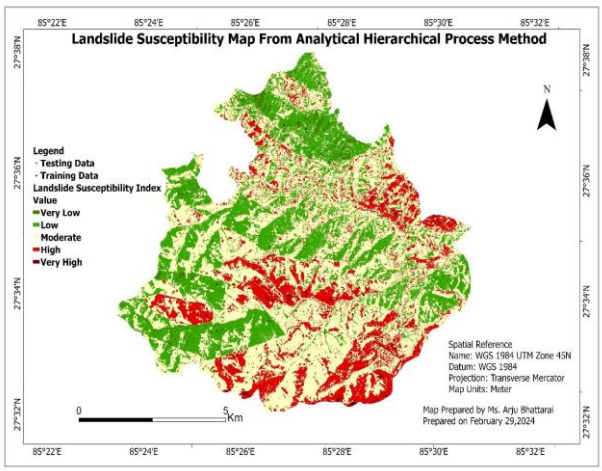

Fig. 15: Landslide susceptible map from AHP method

Analytical Hierarchy Process Method

Landslide Susceptibility Map from AHP Method

LSM was accomplished using the AHP approach as shown in Fig. 15. AHP was used to weight factors and classes as given in Table 5. Raster maps of each factor were weighted on a cell-by-cell basis. Integrating a weighted raster map produced an LSM map containing numerical susceptibility data, with higher LSI values indicating high susceptibility and lower values indicating low susceptibility. LSI values vary from 6.58-37. Now the distribution of landslide susceptibility zones and landslide occurrence is given in Table 6.

In Table 6 maximum class percentage of 52.34 is in the moderate zone, 0.49 which is the lowest percentage in the very high zone.

Frequency Ratio Method

Landslide Susceptibility Map from Frequency Ratio Method

LSM was accomplished using the frequency ratio approach as shown in Fig. 16. Frequency ratio was used to weight factors and classes. Raster maps of each factor were weighted on a cell-by-cell basis. The integration of the weighted raster map produced an LSM map containing numerical susceptibility data, with higher LSI values indicating high susceptibility and lower values indicating low susceptibility. LSI values vary from 356- 1864.

Now the distribution of landslide susceptibility zones and landslide occurrence is given in Table 8.

In Table 8 maximum class percentage of 38.17 is in the moderate zone, 1.01 with the lowest percentage observed in the very high zone.

Table 5: The pair-wise comparison matrix, class weights (rating), and consistency ratio

Matrix		1	2	3	4	5	6	7	8	9	10	weightage %
Slope	1	1	1	1	2	1	1	1	1	1/2	1	9.58
Aspect	2	1	1	1	2	1	4	1	1	2	2	13.19
Lithology	3	1	1	1	4	3	1	1	1	2	4	15.40
LULC	4	1/2	1/2	1/4	1	2	2	1/2	1	2	4	9.92
Distance to fault	5	1	1	1/3	1/2	1	1	2	1	1	4	9.67
Distance to drainage	6	1	1/4	1	1/2	1	1	1	1/3	1	2	7.39
Distance to road network	7	1	1	1	2	1/2	1	1	1	1	4	10.56
Precipitation	8	1	1	1	1	1	3	1	1	1	4	11.44
TWI	9	2	1/2	1/2	1/2	1	1	1	1	1	4	9.21
Curvature	10	1	1/2	1/4	1/4	1/4	1/2	1/4	1/4	1/4	1	3.65

CR = 6.2%

Table 6: The distribution of landslide susceptibility zones and landslide occurrence

Susceptibility classes	Class pixel	Percentage	Landslide pixel	Landslide%	Landslide area
Very low	7532	1.53	9	0.042	937.00
Low	137632	27.89	144	6.008	2261.65
Moderate	258261	52.34	530	25.005	82812.05
High	87568	17.75	1253	59.243	195781.03
Very high	2408	0.49	179	8.463	27968.75
Sum	493401	2115			

Table 7: Frequency ratio of 10 causative factors

Parameters	Classes	Class pixel	% class pixels	Landslide pixels	% landslide pixel)	FR	RF	RF (non%)	RF (Int) RF	Min RF	Max RF	Max-Min	(Max-Min) Min RF	PR
Slope	0-15	066924	13.54	237	11.2500	0.0003	0.016	16.3100	16					
	15-30	185710	37.59	581	27.5800	0.0003	0.014	14.4100	14					
	30-45	189009	38.26	878	41.6900	0.0004	0.0214	21.4000	21					
	45-60	049074	9.93	403	19.1300	0.0008	0.0378	37.8300	37					
	60<	003213	0.65	7	0.3300	0.0002	0.0001	10.0300	10					
Sum		493930	100.00	2106	100.0000	0.0021				0.10	0.37	0.27	0.14	1.94
Aspect	Flat	080292	16.25	82	3.8900	0.0010	0.0022	2.2300	2					
	North	058094	11.75	156	7.4200	0.0026	0.0058	5.8600	5					
	North East	058429	11.82	127	6.0300	0.0021	0.0047	4.7500	4					
	East	062783	12.70	244	11.5800	0.0038	0.0084	8.4940	8					
	South East	049291	9.97	612	29.0500	0.0124	0.0271	27.1300	27					
	South	036695	7.42	645	30.6200	0.0175	0.0384	38.4200	38					
	South West	033404	6.76	135	6.4100	0.0004	0.0088	8.8330	8					
	West	039337	7.96	46	2.1800	0.0001	0.0025	2.5560	2					
	North West	075743	15.33	59	2.8000	0.0007	0.0017	1.7000	1					
Sum		494068	100.00	2106	100.0000	0.045				0.017	0.384	0.367	0.143	2.56
Lithology	Tistung formation	211138	43.20	484	22.8800	0.0002	0.0116	11.6700	11					
	Quaternary deposit	003198	0.65	2	0.0900	0.0006	0.0003	3.1800	3					
	Sopyang formation	37561	7.68	322	15.2200	0.0085	0.0436	43.6500	43					
	Chandragiri formation	183348	37.51	1230	58.1500	0.0067	0.0341	34.1500	34					
	Chitlang formation	53457	10.93	77	3.6400	0.0014	0.0073	7.3300	7					
Sum		488702	100.00	2115	100.0000	0.0196				0.031	0.436	0.404	0.143	2.82
Distance from road	0-1300	435124	87.43	2084	98.7200	0.0047	0.0832	83.2390	83					
	1300-2600	47170	9.47	24	1.1300	0.0005	0.0088	8.8420	8					
	2600-4000	15367	3.08	7	0.3300	0.0004	0.0079	7.9168	7					
Sum		497661	100.00	2115	100.1895	0.0057				0.0791	0.832	0.075	0.143	5.25
Distance from fault	0-1300	326691	72.57	1754	82.9300	0.0005	0.0453	45.3000	45					
	1300-2300	139216	30.92	201	9.5000	0.0001	0.0121	12.1810	12					
	2300<	20407	4.53	160	7.5600	0.0005	0.0425	42.5100	42					
Sum		486314	108.03	2115	100.0000	0.0118				0.121	0.453	0.331	0.143	2.31
Distance from drainage	0-1000	371704	74.81	1636	77.3500	0.0044	0.0512	51.2080	51					
	1000-1500	121037	24.36	478	22.6000	0.0003	0.0459	45.9470	45					
	1500-2500	4086	0.82	1	0.4700	0.0002	0.0028	2.8470	2					
Sum		496827	100.00	2115	100.0000	0.0085				0.028	0.512	0.483	0.143	3.37
Precipitation	1028-1038	90278	18.14	200	9.4560	0.0002	0.0151	15.1010	15					
	1038-1048	251557	50.54	1554	73.4700	0.0006	0.0421	42.1090	42					
	1048-1058	105030	21.10	288	13.6100	0.0020	0.1869	18.6910	18					
	1058-1068	36241	7.28	36	1.7020	0.0009	0.0067	6.7710	6					
	1078-1080	14555	2.92	37	1.7490	0.0250	0.1732	17.3200	17					
Sum		497661	100.00	2115	100.0000	0.1467				0.067	0.421	0.353	0.143	2.46
LULC	Water	19359	2.48	20	0.9400	0.0010	0.0064	0.6400	0					
	Developed	95337	12.26	213	10.0700	0.0020	0.0138	1.3800	1					
	Barren	7821	1.01	1208	57.1100	0.1544	0.9592	95.9200	96					
	Forest	477828	61.45	145	6.8500	0.0003	0.0018	0.1880	1					
	Planted/ cultivated	177173	22.78	529	25.0100	0.0029	0.0185	1.8500	2					
Sum		777518	100.00	2115	100.00	0.1610				0.001	0.959	0.957	0.143	6.67
TWI	0-7	412450	83.48	1872	88.51	0.0045	0.3244	32.4400	32					
	7.0-12	75017	15.18	217	14.57	0.0028	0.2067	20.6700	20					
	12-17.0	6206	1.25	25	3.99	0.0040	0.2879	28.7900	28					
	17-23	395	0.79	1	0.47	0.0025	0.1809	18.0009	18					
Sum		494068		2115		0.0013				0.180	0.324	0.143	0.143	1.00
Curvature	Concave	204502	41.52	1489	70.40	0.0007	0.0770	77.0000	77					
	Convex	288026	58.47	626	29.59	0.0002	0.0229	22.9000	23					
Sum		492528		2115		0.0094				0.229	0.770	0.540	0.143	3.77

Table 8: The distribution of landslide susceptibility zones and landslide occurrence

LSI	LSI pixel	LSI %	Landslide pixel	Landslide %	Landslide area (m^2)
Very low	34256	6.94	8	0.37	1250.00
Low	132040	26.76	166	7.84	25937.05
Moderate	188324	38.17	277	13.09	43281.25
High	133788	27.12	452	21.37	70625.00
Very high	4993	1.01	1212	57.30	189375.00
Sum	493401		2115		

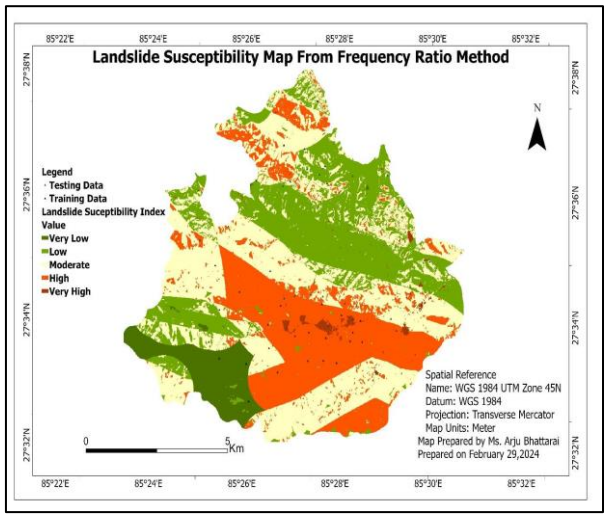

Fig. 16: Landslide susceptible map from frequency ratio method

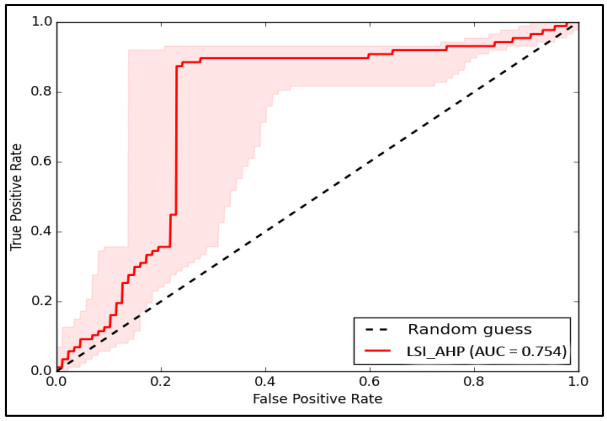

Fig. 17: AUC curve for validation of map from AHP method

Comparison Based on Landslide Density

Landslide density is the area of an existing landslide divided by the area of each landslide susceptibility class. In this study, it is determined based on the number of pixels. In an ideal landslide susceptibility map, the high susceptibility zone should have the maximum landslide density, with the density values dropping gradually from medium to low susceptibility zones.

The landslide densities of the susceptibility classes of both the LSM maps are calculated and tabulated in Table 9.

In the Table 9 for FR, very low LSI class, there are 34,256 pixels and the density of landslide pixels is 0.0002. This means that out of the total pixels classified in the very low LSI class, only a very small proportion (0.02%) are identified as landslide pixels. For AHP, the very low LSI class, there are 7532 pixels and the density of landslide pixels is 0.0012. This means that out of the total pixels classified in the very low LSI class, a small proportion (0.12%) are identified as landslide pixels.

Validation of FR and AHP Method

In Fig. 17 AUC value 0.7547 is achieved for the present model which can be converted in terms of a percent success rate accuracy of 75.47%. So, it can be said that the AHP model gave an accuracy of 75.47%. Additionally, in Fig. 18 AUC value achieved is 0.852. Hence it could be said that the FR model has a high accuracy of 85.2% in comparison to the AHP approach.

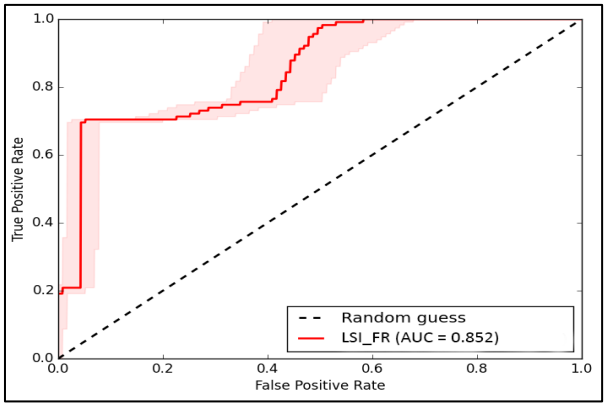

Fig. 18: AUC Curve for validation of map from frequency ratio method

Table 9: The landslide densities of the susceptibility classes of both the LSM maps

	Frequency ratio method			Analytical hierarchical process method		
LSI	Class pixel	Landslide pixel	Density	Class pixel	Landslide Pixel	Density
Very low	34256	8	0.0002	07532	9	0.0012
Low	132040	166	0.0013	137632	144	0.0001
Moderate	188324	277	0.0015	258261	530	0.0021
High	133788	452	0.0034	87568	1253	0.0143
Very high	4993	1212	0.2427	2408	179	0.0743
Sum	493401	2115		493401	2115	

Discussion

The study aimed to identify elements that cause landslides, create a susceptibility map using a geographic information system, and monitor changes using remote sensing techniques. The high and very high susceptibility classes on the weight of the evidence-modeled susceptibility map coincide with steeply sloped areas, i.e., 30-45°. In South Africa also this is no surprise, as slopes greater than 18° are considered susceptible to landslides and therefore not suitable for construction. South-facing slopes have long been more susceptible to landslides (Boelhouwers *et al*., 1998). This was further confirmed in this study when the south-facing slopes recorded the highest number of landslides. The area's geology influences landslides, as different rock types have varying hydrological qualities and strength levels. Geological structures can weaken rocks. It has been noted by Dahal (2014), that lithology is also a major causative factor for inducing landslides. In the study area, Chandragiri formation has the maximum landslide area, the prominent rock found is limestone. Limestone has a high hydraulic transmissivity; higher transmissivity allows water to penetrate deeper into the ground, leading to decreased cohesion of clay minerals and higher pore fluid pressure (Warrick *et al*., 1977). Borrelli *et al*. (2018), also suggest landslides are more prone to occur in locations with faults and lithological connections due to their inherent vulnerability. The fault distance from 0-1300 in the study area consists of maximum landslide pixels. The road network exhibits high and extremely high susceptibility classes in the LSM (Kumar and Anbalagan, 2016). This study analyzed the maximum landslides to be near the road 0-1300 m.

In the LSM map in the Tehri region of Uttarakhand, the results also showed that highly vulnerable classes occupied regions near the drainage network (Kumar and Anbalagan, 2016). Low susceptibility classes are seen in locations with flat terrain, high forest cover, and sparse forest cover. Settlement areas have been classified as somewhat moderate to highly susceptible. The LSM map from this research also provides similar results: Few landslides are seen in forest regions and moderate chances of susceptibility are seen in Built-up areas. Barren slopes are more susceptible to landslides based on field observations and in the LULC map also we could see a maximum number of landslides occurring in barren areas. Slope curvature as a factor (Dahal, 2014) suggests curvatures, along with other parameters, influence water flow in and out of slopes, making them crucial for studying landslides. In this study also maximum landslides above 60% were analyzed to be in concave curvature. The Topographic Wetness Index is a parameter used in terrain analysis to estimate the relative wetness or moisture content of the land surface. It is calculated based on topographic characteristics such as slope and flow accumulation in this study area lower the value of TWI higher the landslide was observed. Maximum landslides were observed in class 0-7 and the landslide percentage decreases higher the value of TWI.

Therefore, selecting an appropriate weighting system was crucial in this study. This study utilized both the weight of evidence and the map combination approach. There are 34,256 pixels in the FR very low LSI class and the density of landslide pixels is 0.0002. This indicates that just a very tiny percentage (0.02%) of all pixels classified in the very low LSI class are identified as landslide pixels. There are 7532 pixels in the very low LSI class AHP and the density of landslide pixels is 0.0012. This indicates that a tiny percentage (0.12%) of all the pixels classified in the very low LSI class are landslide pixels. The difference is seen in the final map too because both are different techniques; one includes weightage whereas another is dependent on the raster cell size of landslides and its factors However, the frequency ratio method outperformed the AHP method in this analysis. The ROC/AUC curve suggests that the accuracy of AHP is about 75% in contrast to the FR which is about 85%. A total of 138 landslides were observed in the study area and plotted into polygons among them 70% were distinguished as training datasets whereas 30% as testing data sets. Testing data sets were used in plotting AUC curves.

Conclusion

LSM was accomplished using the AHP and FR approach. AHP was used to weigh factors and their classifications. The weight values have been given to each factor's raster maps on a cell-by-cell basis in the FR method and for the AHP method multiple; literature review, fieldwork, and consultation with expertise weightage was given to each factor. Integration of weightage to each factor produced an LSI map with numerical susceptibility information, where larger values indicate high susceptibility and lower values indicate low susceptibility. The LSI from AHP method values vary from 6.58-37 Similarly, the LSI value ranges from 356-1864. The continuous LSI map from both methods was divided into 5 groups using the natural break classifier. There are 5 levels of susceptibility: Very low, low, moderate, high, and extremely high. From the result of both the maps a maximum region of the study area has moderate chances of landslide i.e., about 58% of the study area is susceptible to landslide from AHP in contradiction to the FR method about 48% of the total area has moderate chances similarly in FR method 27% of the area is susceptible to landslide whereas AHP method provides 22% of predication. However, the map presented by AHP and FR both is recommendable because the success rate of AHP is about 75% and FR is 85%. The first stage in planning for future land use is to assess the requirement for landslide susceptibility information to avoid exceeding an

acceptable level of risk. Landslide risk refers to the degree of loss caused by a certain landslide. Landslide information aims to identify regions vulnerable to landslides and recommend appropriate development measures. Landslides can disrupt human activities and the economy. Understanding the area's landslide risk is vital. Landslide susceptibility maps only show locations with a high likelihood of landslides, not when they may occur. Planners can use these estimations to make decisions about site suitability, kind of development, and mitigation measures.

Acknowledgment

Special thanks to my supervisor, Dr. Him Lal Shrestha, for his invaluable guidance, encouragement, and dedication throughout my research. I also sincerely thank Panauti Municipality for their financial support and motivation during my thesis work. I am thankful to my colleagues, Ms. Anushka Gyawali, Mr. Asim Timalsina, Mr. Sujan Bista and Mr. Kishor Rimal, for their support. Finally, I am forever grateful to my parents for their unwavering encouragement and for creating a supportive environment for my studies.

Funding Information

"This research was funded by Panauti Municipality, Nepal, under a research grant for studying the landslide-prone Nagi Dada area, which is evolving as a tourism destination and requires serious investigation."

Author's Contributions

Arju Bhattarai: Conducted field visits, performed data analysis, created maps and finalized the report.

Himlal Shrestha: Provided guidance, developed the concept, and reviewed the work.

Asim Timalsina, Sujan Bista, Kishor Rimal and Anushka Gywali: Participated in field visits.

Ethics

By signing below, we affirm that this thesis report is solely the product of my own efforts. We have appropriately cited all sources of information and data utilized in my research and have clearly indicated their origins.

References

Bhandari, R. K., & Upreti, B. N. (2015). Geological investigation of landslides in the northern part of Kavrepalanchok District Central Nepal. *Journal of Nepal Geological Society*, *49*, 15–22.

Boelhouwers, J., Duiker, J. M. C., & Van Duffelen, E. A. (1998). Spatial, morphological and sedimentological aspects of recent debris flows in Du Toit's Kloof, Western Cape. *South African Journal of Geology*, *101*(1), 73–89.

Borrelli, L., Ciurleo, M., & Gullà, G. (2018). Shallow landslide susceptibility assessment in granitic rocks using GIS-based statistical methods: the contribution of the weathering grade map. *Landslides*, *15*(6), 1127–1142. https://doi.org/10.1007/s10346-018-0947-7

Chang, Z., Catani, F., Huang, F., Liu, G., Meena, S. R., Huang, J., & Zhou, C. (2023). Landslide susceptibility prediction using slope unit-based machine learning models considering the heterogeneity of conditioning factors. *Journal of Rock Mechanics and Geotechnical Engineering*, *15*(5), 1127–1143. https://doi.org/10.1016/j.jrmge.2022.07.009

Cruden, D. M. (1991). A simple definition of a landslide. *Bulletin of the International Association of Engineering Geology*, *43*(1), 27–29. https://doi.org/10.1007/bf02590167

Dahal, R. K. (2014). Regional-scale landslide activity and landslide susceptibility zonation in the Nepal Himalaya. *Environmental Earth Sciences*, *71*(12), 5145–5164. https://doi.org/10.1007/s12665-013-2917-7

Ehret, D., Rohn, J., Dumperth, C., Eckstein, S., Ernstberger, S., Otte, K., Rudolph, R., Wiedenmann, J., Xiang, W., & Bi, R. (2010). Frequency ratio analysis of mass movements in the Xiangxi catchment, Three Gorges Reservoir area, China. *Journal of Earth Science*, *21*(6), 824–834. https://doi.org/10.1007/s12583-010-0134-9

El Jazouli, A., Barakat, A., & Khellouk, R. (2019). GIS-multicriteria evaluation using AHP for landslide susceptibility mapping in Oum Er Rbia high basin (Morocco). *Geoenvironmental Disasters*, *6*(1), 1–12. https://doi.org/10.1186/s40677-019-0119-7

Ghosh, S., Kumar, A., & Bora, A. (2014). Analyzing the stability of a failing rock slope for suggesting suitable mitigation measure: a case study from the Theng rockslide, Sikkim Himalayas, India. *Bulletin of Engineering Geology and the Environment*, *73*(4), 931–945. https://doi.org/10.1007/s10064-014-0586-8

Hasegawa, S., Dahal, R. K., Yamanaka, M., Bhandary, N. P., Yatabe, R., & Inagaki, H. (2009). Causes of large-scale landslides in the Lesser Himalaya of central Nepal. *Environmental Geology*, *57*(6), 1423–1434. https://doi.org/10.1007/s00254-008-1420-z

Hasekioğulları, G. D., & Ercanoglu, M. (2012). A new approach to use AHP in landslide susceptibility mapping: a case study at Yenice (Karabuk, NW Turkey). *Natural Hazards*, *63*(2), 1157–1179. https://doi.org/10.1007/s11069-012-0218-1

Hoo, Z. H., Candlish, J., & Teare, D. (2017). What is an ROC curve? *Emergency Medicine Journal*, *34*(6), 357–359. https://doi.org/10.1136/emermed-2017-206735

Kanungo, D. P., Arora, M. K., Sarkar, S., & Gupta, R. P. (2009). A fuzzy set based approach for integration of thematic maps for landslide susceptibility zonation. *Georisk: Assessment and Management of Risk for Engineered Systems and Geohazards*, *3*(1), 30–43. https://doi.org/10.1080/17499510802541417

Kumar, R., & Anbalagan, R. (2016). Landslide susceptibility mapping using Analytical Hierarchy Process (AHP) in Tehri reservoir rim region, Uttarakhand. *Journal of the Geological Society of India*, *87*(3), 271–286. https://doi.org/10.1007/s12594-016-0395-8

Li, T. (1992). *Landslide Hazards and their Mitigation in China* (1st Ed.). Science Press.

Mondal, S., & Maiti, R. (2013). Integrating the Analytical Hierarchy Process (AHP) and the Frequency Ratio (FR) model in landslide susceptibility mapping of Shiv-khola watershed, Darjeeling Himalaya. *International Journal of Disaster Risk Science*, *4*(4), 200–212. https://doi.org/10.1007/s13753-013-0021-y

Paudel, P. N., & Tamrakar, N. K. (2013). Geology and rockmass condition of Dhulikhel-Panchkhal area, Kavre District, Central Nepal Lesser Himalaya. *Bulletin of the Department of Geology*, *15*, 1–14. https://doi.org/10.3126/bdg.v15i0.7412

Rusydy, I., Al-Huda, N., Fahmi, M., & Effendi, N. (2019). Kinematic Analysis and Rock Mass Classifications for Rock Slope Failure at USAID Highways. *Structural Durability and Health Monitoring*, *13*(4), 379–398. https://doi.org/10.32604/sdhm.2019.08192

Saaty, T. L., & Vargas, L. G. (2001). The Seven Pillars of the Analytic Hierarchy Process. In *Models, Methods, Concepts & Applications of the Analytic Hierarchy Process* (*Vol. 34*, pp. 27–46). Springer. https://doi.org/10.1007/978-1-4615-1665-1_2

Stöcklin, J., & Bhattarai, K. D. (1977). *Geology of Kathmandu area and Central Mahabharat range: Nepal Himalaya*. HMG/UNDP mineral exploration project.

Van Der Geest, K. E. E. S., & Schindler, M. A. R. K. U. S. (2016). *Case study report: Loss and damage from a catastrophic landslide in Sindhupalchok District, Nepal*. Bonn: Institute for Environment and Human Security, United Nations University.

Varnes, D. J. (1978). Slope movements: Types and processes. *Transportation Research Board Special Report*, 11–33.

Warrick, A. W., Mullen, G. J., & Nielsen, D. R. (1977). Scaling field-measured soil hydraulic properties using a similar media concept. *Water Resources Research*, *13*(2), 355–362. https://doi.org/10.1029/wr013i002p00355

Yalcin, A. (2007). Environmental Impacts of Landslides: A Case Study from East Black Sea Region, Turkey. *Environmental Engineering Science*, *24*(6), 821–833. https://doi.org/10.1089/ees.2006.0161

Yalcin, A. (2008). GIS-based landslide susceptibility mapping using analytical hierarchy process and bivariate statistics in Ardesen (Turkey): Comparisons of results and confirmations. *CATENA*, *72*(1), 1–12. https://doi.org/10.1016/j.catena.2007.01.003

Yalcin, A., Reis, S., Aydinoglu, A. C., & Yomralioglu, T. (2011). A GIS-based comparative study of frequency ratio, analytical hierarchy process, bivariate statistics and logistics regression methods for landslide susceptibility mapping in Trabzon, NE Turkey. *CATENA*, *85*(3), 274–287. https://doi.org/10.1016/j.catena.2011.01.014